An Examination of Several Methods of Hyperspectral Image Denoising: Over Channels, Spectral Functions and Both Domains

Daniel Otero[1(✉)], Oleg V. Michailovich[2], and Edward R. Vrscay[1]

[1] Department of Applied Mathematics, Faculty of Mathematics, University of Waterloo, Waterloo, ON N2L 3G1, Canada
[2] Department of Electrical and Computer Engineering, Faculty of Engineering, University of Waterloo, Waterloo, ON N2L 3G1, Canada
{dotero,olegm,ervrscay}@uwaterloo.ca

Abstract. The corruption of hyperspectral images by noise can compromise tasks such as classification, target detection and material mapping. For this reason, many methods have been proposed to recover, as best as possible, the uncorrupted hyperspectral data from a given noisy observation. In this paper, we propose and compare the results of four denoising methods which differ in the way the hyperspectral data is treated: (i) as 3D data sets, (ii) as collections of frequency bands and (iii) as collections of spectral functions. In the case of additive noise, these methods can be easily adapted to accommodate different degradation models. Our methods and results help to address the question of how hyperspectral data sets should be processed in order to obtain useful denoising results.

1 Introduction

In this paper we consider the problem of denoising digital hyperspectral (HS) images obtained from remote sensing of the earth's surface. In this case, the HS image associated with a given surface region R is comprised of a set of reflectance values – ratios of reflected energy vs. incident energy – of electromagnetic radiation at a number of frequencies (or, equivalently, wavelengths) at each pixel location in R. The number of frequencies depends upon the spectral resolution of the sensor of the hyperspectral camera and may range from tens to hundreds. For example, the well-known AVIRIS (Airborne Visible/Infrared Imaging Spectrometer) satellite images [1] typically contain 224 frequencies.

Suppose that a region R of the earth's surface is represented by an $M \times N$ pixel array and that associated with each pixel in the array there are P reflectance values. The first, and most obvious, way of viewing this HS data set is as a $M \times N \times P$ "data cube." The correlations between neighbouring entries of this cube give rise to two additional and complementary ways of viewing this 3D data set: (ii) as a collection of P images of region R at different frequencies – often referred to as *spectral channels* or *frequency/wavelength bands* – and

A. Campilho and M. Kamel (Eds.): ICIAR 2014, Part I, LNCS 8814, pp. 131–140, 2014.
DOI: 10.1007/978-3-319-11758-4_15

(iii) as a collection of $M \times N$ P-vectors, each of which corresponds to a given pixel location (i, j) of R – often referred to as the *spectral function* or, simply, *spectrum* at (i, j). These three views of the HS image will play a central theme in this paper.

Let us very briefly recall the importance of spectral functions. Since different materials, e.g., minerals, water, vegetation, exhibit different reflectance spectra, the latter serve as "spectral fingerprints". The spectrum at a pixel (i, j) makes it possible to determine the composition/nature of material situated at that location. This makes the study of HS images useful in a variety of applications, including agriculture, mineralogy, geography and surveillance, the latter involving hyperspectral imaging tasks such as target detection and classification [23]. In light of the acquisition process, HS images are, as in the case of many other images, prone to contamination by noise which can compromise the performance of such tasks. As a result, it is desirable to develop reconstruction techniques that recover good approximations of noise-free HS images.

Indeed, many different methods for denoising HS data have been proposed. For example, in [18], diffusion-based filtering is adapted to HS images. The proposed method consists of two diffusion processes, one confined to each band of the HS image, and the another restricted to the spectral domain. The overall anisotropic diffusion is basically a combination of these two processes, which are carried out in a controlled fashion. In [19], a rather novel wavelet-based denoising approach is proposed. This method transforms the HS data set into a spectral-derivative domain, in which the irregularity of noise is more easily detected. The transformed HS image is denoised using wavelet shrinkage (WS) independently in both the spatial and spectral domains. A reconstruction is then obtained by first computing the corresponding inverse wavelet transforms of the denoised data followed by an integration in the spectral direction. Another method that carries out denoising employing WS is presented in [9]. Here, principal component analysis (PCA) is used to decorrelate the most relevant HS data from the noise, most of which is assumed to be contained in the lowest energy components of the transformed data. The noise is removed from these components using WS in both spatial and spectral domains. The denoised HS data set is then retrieved by means of the inverse PCA transform. Variational approaches are proposed in [8,26]. In [26], a total variation (TV) model that considers the changes of noise intensity present across the bands and pixels of an HS image is proposed. In [8], a method that employs a TV model along with sparse representations of each band is also introduced. More approaches can also be found in [20,21].

In this study, we wish to examine the roles of both spatial (pixel) and spectral domains in the denoising of HS images. For example, is it preferable to focus the denoising in one domain at the expense of the other, or should both domains be considered? In order to shed some light on this and related questions, we compare four different denoising approaches. The main difference between these approaches lies in the way that the HS image is treated, using the three views mentioned earlier, i.e., as a (i) 3D data "cube", (ii) a set of frequency bands or (iii) a set of spectral functions.

In our first approach, the denoising process is performed in the spectral domain, corresponding to (iii) above. In particular, we apply ℓ_1-norm regularization [2,17,24] to the spectral functions. In the second approach, the denoising process is performed in the spatial domain, corresponding to (ii) above. As expected, any denoising technique applicable to 2D signals/images can be employed – here, we focus our attention on the TV approach [6,22]. Our third approach employs a formulation of vectorial TV to denoise the entire HS image at once [5,14], corresponding to (i) above. Finally, in our fourth approach, an HS image is viewed as a collection of both spectra and frequency bands. Our method involves a combination of the first two approaches so that denoising is carried out by regularization in both the spatial and spectral domains. To solve this inverse problem we employ the Alternating Direction Method of Multipliers (ADMM) [4]. Experimental results are then presented so that the performance of these methods can be compared.

2 Denoising

In practice, the strengths of the denoising process across spatial and spectral domains of an HS image should be different. Even within the spatial domain, different features such as edges and flat regions should not be denoised with the same intensity. In addition, it is quite common that the power of noise across bands is not constant [3,26]. Some methods that address these possible scenarios can be found in the literature, e.g., [19,26]. Nevertheless, in this study, for the sake of simplicity we assume that the power of the noise is constant over the entire HS data set, i.e., it is independent of the location and band of a given voxel. As such, we consider the following simple degradation model,

$$f = u + n, \tag{1}$$

where f is the noisy observation, u is the noiseless HS data we wish to recover, and n is additive white Gaussian noise (AWGN). In this case, f, n and u are considered as $M \times N \times P$ HS data cubes. Moreover, for the remainder of the paper, this interpretation of HS images as 3D discrete data sets is the one that we will consider, unless otherwise stated.

Despite that Eq. (1) may not always be a proper model for noise in HS images, it will be seen that some of the methods presented below can be easily adapted for different scenarios in which the noise characteristics change over space and wavelength.

2.1 Denoising of Hyperspectral Images as a Collection of Spectra

Here we view f as a collection of P spectra. The problem is therefore split into $M \times N$ subproblems, with the denoising being carried out in the spectral direction on each of the P spectral functions.

Each spectral function may be denoised with any of the available denoising techniques that can be applied to 1D signals, e.g., wavelet shrinkage, linear filtering, 1D total variation denoising, etc.. Here, however, we investigate the effectiveness of ℓ_1-norm regularization, primarily because of the good performance of methods that exploit sparse representations of signals [2,17,24].

In this approach, we solve the following sparse approximation problem independently at each pixel (i, j),

$$\min_{c_{ij}} \left\{ \frac{1}{2} \|Dc_{ij} - s_{ij}\|_2^2 + \lambda \|c_{ij}\|_1 \right\}, \tag{2}$$

where s_{ij} denotes the noisy spectrum, D is an appropriate transformation matrix (e.g., frame, random matrix, etc.), and c_{ij} is the set of coefficients that is to be recovered at the pixel location (i, j).

In the literature, many algorithms for solving (2) can be found [2,17,24], however, we focus our attention on the special case in which the matrix D is an orthogonal transformation (e.g., DCT, wavelet transform, Fourier matrix, etc.). In this particular case, problem (2) can be solved by means of the soft thresholding (ST) operator [4,24].

It is worth pointing out that this approach allows us to change the strength of the denoising process across the spatial domain, i.e., different regularization parameters can be used at different pixels or in different regions of the HS image.

2.2 Denoising of Hyperspectral Images as a Collection of Bands

In this approach, the denoising process takes place in the spatial domain. Each frequency/wavelength band is treated independently and the denoising problem is split into P independent subproblems. Here, we consider each k-th band u_k as a scalar function $u_k : \Omega \to \mathbb{R}$, where $\Omega \subset \mathbb{R}^2$ and $1 \leq k \leq P$.

As expected, any denoising method for 2D images can be employed here, e.g., linear filtering, non-local means denoising, total variation, non-linear filtering, etc.. Nevertheless, in this study, we employed a TV denoising approach for which a number of fast algorithms exist, e.g., [6,15,22]. As well, some TV-based denoising methods for HS images have yielded promising results [8,26].

Our approach, a channel-by-channel TV method in the spatial domain where each band u_k is treated independently, translates to the following approximation problem,

$$\min_{u_k} \left\{ \frac{1}{2\mu} \|u_k - f_k\|_2^2 + \|u_k\|_{TV} \right\}, \tag{3}$$

where $\|\cdot\|_{TV}$ is the total variation norm and f_k is the k-th noisy band or channel. To solve this problem numerically, we employ the method introduced by Chambolle in [6], which has received special attention because of its excellent performance. Here, the following definition of the isotropic TV norm is employed,

$$\|u_k\|_{TV} = \int_\Omega \|Du_k\|_2 dxdy = \sup_{\xi_k \in \Xi_k} \left\{ \int_\Omega u_k \nabla \cdot \xi_k \, dxdy \right\}, \tag{4}$$

where $\Xi_k = \{\xi_k : \xi_k \in C_c^1(\Omega, \mathbb{R}^2), \|\xi_k(x)\|_2 \leq 1 \ \forall x \in \Omega\}$, and $\nabla\cdot$ is the divergence operator. If $u_k \in C_c^1(\Omega, \mathbb{R})$, $Du_k = \nabla u_k$ in the distributional sense. This approach is convenient since only the integrability, and not the differentiability, of u_k is required.

By using (4), Chambolle shows that the optimal solution $u_k^\star$ of (3) is given by $u_k^\star = f_k - \Pi_{\mu\Gamma_k}(f_k)$, where $\Pi_{\mu\Gamma_k}(f_k)$ is the non-linear projection of f_k onto the convex set $\mu\Gamma_k$, and Γ_k is the closure of the set $\{\nabla \cdot \xi_k : \xi_k \in C_c^1(\Omega, \mathbb{R}^2), \|\xi_k(x)\|_2 \leq 1 \ \forall x \in \Omega\}$. Such projection is obtained by solving the following minimization problem:

$$\min_{\|\xi_k(x)\|_2 \leq 1} \{\mu\nabla \cdot \xi_k - f_k\}. \tag{5}$$

Thus, we have that for each band the optimal reconstruction is given by $u_k^\star = f_k - \mu\nabla \cdot \xi_k^\star$.

This approach may easily be modified to accommodate the case in which the power of the noise is not constant throughout the bands. In this case, one can specify the degree of regularization to be applied to each channel independently by means of the parameter μ.

2.3 Denoising of Hyperspectral Images as a Whole

In this case, we view a HS image as a vector-valued function $u : \Omega \to \mathbb{R}^P$, where $\Omega \subset \mathbb{R}^2$. To denoise it, we follow a variational approach, employing a definition of the Vectorial TV seminorm (VTV).

Given the effectiveness of TV for denoising images – along with its applicability to other image processing tasks such as inpainting, zooming, etc. – many extensions for vector-valued functions have been proposed [5,14]. Indeed, a practical application already exists for colour images, which are essentially low-dimensional HS images. This approach can easily be extended to HS images, with no required changes to the definitions presented in the literature. In particular, we use Bresson and Chan's approach [5], which is a generalization of Chambolle's algorithm for vector-valued functions. Here, the authors extend the Rudin-Osher-Fatemi model [22] as follows,

$$\min_u \left\{ \frac{1}{2\mu}\|u - f\|^2_{L_2(\Omega;\mathbb{R}^P)} + \|u\|_{VTV} \right\}, \tag{6}$$

where f is the noisy observation. The VTV seminorm is defined as

$$\|u\|_{VTV} = \int_\Omega \|Du\| d\mathbf{x} = \sup_{\xi \in \boldsymbol{\Xi}} \left\{ \int_\Omega \langle u, \nabla \cdot \xi \rangle d\mathbf{x} \right\}; \tag{7}$$

where $\boldsymbol{\Xi} = \{\xi : \xi \in C_c^1(\Omega, \mathbb{R}^{2\times P}), \|\xi(\mathbf{x})\|_2 \leq 1 \ \forall \mathbf{x} \in \Omega\}$; $\langle\cdot,\cdot\rangle$ is the standard Euclidean scalar product in $\mathbb{R}^P$; and $\|Du\|^2 = \sum_{k=1}^P \|\nabla u_k\|_2^2$ if $u \in C_c^1(\Omega, \mathbb{R}^P)$, that is, the ℓ_2 norm of the TV norm of all the bands u_k of the HS image u.

Substitution of (7) into (6) yields to the following minimization problem:

$$\min_{\|\xi(\mathbf{x})\|_2 \leq 1} \left\{ \left\| \nabla \cdot \xi - \frac{f}{\mu} \right\|^2_{L_2(\Omega;\mathbb{R}^P)} \right\}, \tag{8}$$

whose solution $\xi^\star$ is computed using a semi-implicit gradient descent scheme. The solution $u^\star$ of the original problem in (6) is obtained using $u^\star = f - \mu \nabla \cdot \xi^\star$. In our case, f is the noisy HS image.

2.4 Denoising of Hyperspectral Images a Collection of Both Bands and Spectra

In this fourth approach, we perform regularization in both the spectral and spatial domains. This can be done in various ways, but we focus our attention on the methods employed previously, that is, TV- and ℓ_1-norm regularization.

As expected, denoising in the spectral domain is carried out by solving an optimization problem in which the ℓ_1 norm of a set of coefficients is used as a regularizing term. Denoising in the spatial domain is performed using a variational approach. In other words, we consider a good reconstruction of the original HS data u from the noisy observation f to be one with bounded variation across bands and with spectral functions that possess sparse representations in a certain domain. In order to find such a reconstruction, we solve the following optimization problem,

$$\min_c \left\{ \frac{1}{2} \|S(c) - f\|_2^2 + \mu \|S(c)\|_{VTV} + \lambda \|c\|_1 \right\}, \tag{9}$$

where $S(\cdot)$ is a synthesis operator that reconstructs the HS image from the set of coefficients c. More specifically, at each pixel (i, j), the operator $S(\cdot)$ recovers the spectrum located at that pixel location by computing Dc_{ij}, where c_{ij} is the set of coefficients associated to such spectrum.

For solving problem (9) we employ ADMM, which is a method well suited for convex optimization and large scale problems [4]. We first need to express (9) in ADMM form:

$$\begin{gathered} \min_{c,u} \left\{ \tfrac{1}{2} \|u - f\|_2^2 + \mu \|u\|_{VTV} + \lambda \|c\|_1 \right\} \\ \text{subject to } S(c) - u = 0. \end{gathered} \tag{10}$$

It is well known [4] that this new problem can be solved by forming the augmented Lagrangian and minimizing with respect to the variables c and u in an alternate fashion. Given this, we propose the following ADMM iterations for solving (9):

$$c^{n+1} := \min_c \left\{ \frac{1}{2} \left\| S(c) - \frac{f + \delta(u^n - p^n)}{\delta + 1} \right\|_2^2 + \frac{\lambda}{\delta + 1} \|c\|_1 \right\} \tag{11}$$

$$u^{n+1} := \min_u \left\{ \frac{\delta}{2\mu} \|u - (S(c^{n+1}) + p^n)\|_2^2 + \|u\|_{VTV} \right\} \tag{12}$$

$$p^{n+1} := p^n + S(c^{n+1}) - u^{n+1}, \tag{13}$$

where p is the dual variable associated to the augmented Lagrangian, (13) its update, and δ is a penalty parameter. Problem (11) can be solved by any algorithm capable of carrying out sparse reconstruction using the ℓ_1 norm as a regularizing term. Problem (12) can be addressed using any method employing the vectorial TV norm. In particular, we have used ST to solve (11) at each pixel and Bresson and Chan's algorithm for problem (12).

It is important to mention that different regularization terms can be used in problem (11) since it is solved at each pixel independently. Moreover, problem (12) can be solved using our second approach in Section 2.2, that is, denoising each band independently, in which case the regularization can be changed from band to band. In other words, our fourth approach may be adapted for denoising with different intensities across both spatial as well as spectral domains.

3 Experiments

In order to compare the performance of the four methods described above, they were applied to noisy versions of the Indian Pines and Salinas-A HS images. The latter is a subset of the Salinas HS image – both of them can be downloaded from [16]. The sizes of the 3D Indian Pines and Salinas-A data sets are $145 \times 145 \times 220$ and $83 \times 86 \times 224$, respectively. White additive Gaussian noise was added to these HS data (assumed to be noiseless). In all experiments, the Peak Signal-to-Noise Ratio (PSNR) before denoising was 30.103 dB.

In the approaches where a set of optimal coefficients was to be determined, the transformation matrix D employed was the Karhunen-Loève Transform (KLT), which was computed for each HS image. The KLT was chosen since it gives a very sparse representation of the HS data (as compared to DCT, wavelet and other transforms), as well as being optimal in the ℓ_2 sense. When the KLT is used, the mean of the HS data must be subtracted prior to processing.

As for measures of performance, we employed the Mean Square Error (MSE), PSNR, and the Structural Similarity Index Measure (SSIM) [25]. For the latter, we computed the SSIM between the original and recovered HS images in both the spatial and spectral domains. For the spatial case, the SSIM is computed between bands; whereas in the spectral case, the SSIM is computed between spectra. An overall SSIM is obtained by simply averaging all the computed SSIMs for both the spatial and the spectral cases. Observe that the greater the similarity between two images, the closer their SSIM is to 1. In Table 1, a summary of these quantitative results is shown.

According to these results, the fourth approach (ADMM) outperforms all the other methods respect to any of the metrics of performance that were considered. Only in the denoising results for Indian Pines, the spectral-oriented method described in section 2.1 is as good as ADMM in the "spectral-SSIM sense". The latter suggests that methods that carry out regularization in both the spectral and spatial domains may perform better than methods in which the denoising process is not carried out in this fashion. We believe this to be the case because the fourth approach captures best the "nature" of HS data, that is, data that is correlated in both the spatial and spectral domains.

For visual comparison, some results are presented in Figures 1 and 2. Figure 1 demonstrates how the methods achieve the denoising in the spatial domain. The SSIM maps, shown in the top row of Figure 1, illustrate the similarity between the reconstructions (denoised) and the original (noiseless) HS data for a particular band. The brightness of these maps is an indication of the magnitude of the local SSIM, i.e., the brighter a given location the greater the similarity between the retrieved and the original bands at that point [25]. Figure 2 shows the denoising yielded by different methods in the spectral domain.

Table 1. Numerical results for the different approaches. Numbers in bold identify the best results with respect to each of the four measures of performance considered. In all cases, the PSNR prior to denoising was 30.103 dB.

SALINAS-A				
	ST	TV	VTV	ADMM
MSE	4860.8284	4944.6999	4853.3592	**4218.4193**
PSNR (dB)	41.5905	41.5162	41.5972	**42.2061**
SPATIAL SSIM	0.9812	0.9575	0.9658	**0.9855**
SPECTRAL SSIM	0.9977	0.9977	0.9979	**0.9980**
INDIAN PINES				
MSE	13803.4370	15516.8153	18415.5653	**13268.2362**
PSNR (dB)	38.2492	37.7410	36.9972	**38.3046**
SPATIAL SSIM	0.9533	0.9338	0.9132	**0.9556**
SPECTRAL SSIM	**0.9972**	0.9970	0.9963	**0.9972**

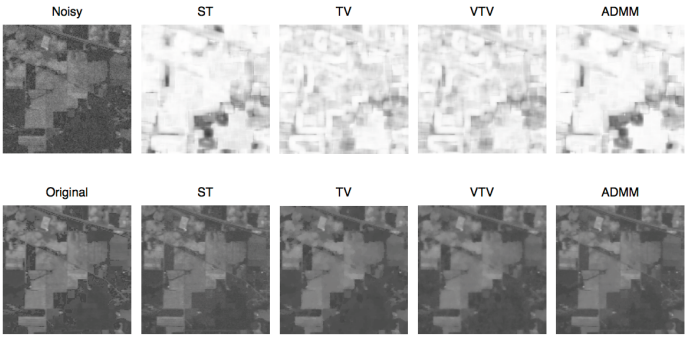

Fig. 1. Visual results for Band No. 23 of the Indian Pines HS image. Beside the original (noiseless) image in the lower row are shown the various reconstruction results. Beside the noisy image in the upper row are shown the corresponding SSIM maps between the reconstructed (denoised) images and the original image.

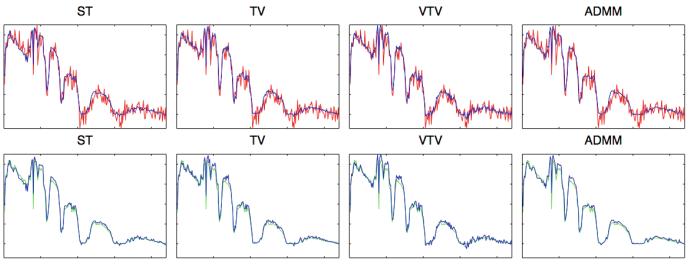

Fig. 2. Denoising results for a particular spectral function of the Indian Pines HS image. Plots in green, blue and red correspond to the original, recovered and noisy spectra, respectively.

Acknowledgments. We gratefully acknowledge that this research was supported in part by the Natural Sciences and Engineering Research Council (NSERC).

References

1. AVIRIS website: http://aviris.jpl.nasa.gov/index.html
2. Amir Beck, A., Teboulle, M.: A fast iterative shrinkage-thresholding algorithm for linear inverse problems. SIAM Journal on Imaging Sciences Archive **2**(1), 183–202 (2009)
3. Bioucas-Dias, J.M., Nascimento, J.M.P.: Hyperspectral Subspace Identification. IEEE Trans. Geoscience and Remote Sensing **46**, 2435–2445 (2008)
4. Boyd, S.P., Parikh, N., Chu, E., Peleato, B., Eckstein, J.: Distributed Optimization and Statistical Learning via the Alternating Direction Method of Multipliers. Foundations and Trends in Machine Learning **3**, 1–122 (2011)
5. Bresson, X., Chan, T.: Fast Dual Minimization of the Vectorial Total Variation Norm and Applications to Color Image Processing. Inverse Problems and Imaging **2**(4), 455–484 (2008)
6. Chambolle, A.: An algorithm for total variation minimization and applications. Journal of Mathematical Imaging and Vision **20**(1–2), 89–97 (2004)
7. Chan, T., Shen, J.: Image Processing and Analysis. Society for Industrial and Applied Mathematics, Philadelphia (2005)
8. Chang, Y., Yan, L., Fang, H., Liu, H.: Simultaneous Destriping and Denoising for Remote Sensing Images With Unidirectional Total Variation and Sparse Representation. IEEE Geoscience and Remote Sensing Letters **11**(6), 1051–1055 (2014)
9. Chen, G., Qian, S.E.: Denoising of Hyperspectral Imagery Using Principal Component Analysis and Wavelet Shrinkage. IEEE Trans. Geoscience and Remote Sensing **49**, 973–980 (2011)
10. Donoho, D.: Denoising by Soft-Thresholding. IEEE Trans. Information Theory **41**(3), 613–627 (1995)
11. Donoho, D., Johnstone, I.M.: Adapting to Unknown Smoothness Via Wavelet Shrinkage. J. of the Amer. Stat. Assoc. **90**(432), 1220–1224 (1995)
12. Donoho, D., Johnstone, I.M., Kerkyacharian, G., Picard, D.: Wavelet shrinkage: asymptopia. Journal of the Royal Statistical Society, Ser. B, 371–394 (1995)
13. Elad, M., Aharon, M.: Image denoising via sparse and redundant representations over learned dictionaries. IEEE Trans. Image Proc. **15**(12), 3736–3745 (2006)

14. Goldlücke, B., Strekalovskiy, E., Cremers, D.: The Natural Vectorial Total Variation Which Arises from Geometric Measure Theory. SIAM J. Imaging Sciences **5**, 537–563 (2012)
15. Goldstein, T., Osher, S.: The Split Bregman Method for ℓ_1-Regularized Problems. SIAM J. Imaging Sciences **2**, 323–343 (2009)
16. http://www.ehu.es/ccwintco/index.php/Hyperspectral_Remote_Sensing_Scenes
17. Mairal, J., Bach, F., Jenatton, R., Obozinski, G.: Convex Optimization with Sparsity-Inducing Norms. Optimization for Machine Learning. MIT Press (2011)
18. Martín-Herrero, J.: Anisotropic Diffusion in the Hypercube. IEEE Trans. Geoscience and Remote Sensing **45**, 1386–1398 (2007)
19. Othman, H., Qian, S.E.: Noise Reduction of Hyperspectral Imagery Using Hybrid Spatial-Spectral Derivative-Domain Wavelet Shrinkage. IEEE Trans. Geoscience and Remote Sensing **44**, 397–408 (2006)
20. Renard, N., Bourennane, S., Blanc-Talon, J.: Denoising and Dimensionality Reduction Using Multilinear Tools for Hyperspectral Images. IEEE Geoscience and Remote Sensing Letters **5**(2), 138–142 (2008)
21. Rasti, B., Sveinsson, J.R., Ulfarsson, M.O., Benediktsson, J.A.: Hyperspectral image denoising using 3D wavelets. In: 2012 IEEE International Geoscience and Remote Sensing Symposium (IGARSS), pp. 1349–1352 (2012)
22. Rudin, L., Osher, S., Fatemi, E.: Nonlinear total variation based noise removal algorithms. Physica D: Nonlinear Phenomena **60**(1–4), 259–268 (1992)
23. Shippert, P.: Why use Hyperspectral imaging? Photogrammetric Engineering and Remote Sensing, 377–380 (2004)
24. Turlach, B.A.: On algorithms for solving least squares problems under an ℓ_1 penalty or an ℓ_1 constraint. In: Proceedings of the American Statistical Association, Statistical Computing Section, pp. 2572–2577 (2005)
25. Wang, Z., Bovik, A.C., Sheikh, H.R., Simoncelli, E.P.: Image Quality Assessment: from Error Visibility to Structural Similarity. IEEE Trans. Image Processing **13**, 600–612 (2004)
26. Yuan, Q., Zhang, L., Shen, H.: Hyperspectral Image Denoising Employing a Spectral-Spatial Adaptive Total Variation Model. IEEE Trans. Geoscience and Remote Sensing **50**, 3660–3677 (2012)